Journal of The Electrochemical Society

The Electrochemical Society
Advancing solid state & electrochemical science & technology

OPEN ACCESS

Electrokinetic Streaming Current Method to Probe Polycrystalline Gold Electrode-Electrolyte Interface Under Applied Potentials

To cite this article: Prantik Saha and Iryna V. Zenyuk 2021 *J. Electrochem. Soc.* **168** 046511

View the article online for updates and enhancements.

This content was downloaded from IP address 98.164.252.236 on 28/04/2021 at 07:20

Journal of The Electrochemical Society, 2021 **168** 046511

Electrokinetic Streaming Current Method to Probe Polycrystalline Gold Electrode-Electrolyte Interface Under Applied Potentials

Prantik Saha[1,2] and **Iryna V. Zenyuk**[2,3,z]

[1]*Department of Physics & Astronomy, University of California Irvine, Irvine, California 92617, United States of America*
[2]*National Fuel Cell Research Center (NFCRC), University of California Irvine, Irvine, California 92697, United States of America*
[3]*Department of Chemical and Biomolecular Engineering, University of California Irvine, Irvine, California 92617, United States of America*

We developed a method, by combining electrochemical and electrokinetic streaming current techniques to study ion distribution and ionic conductivity in the diffuse part of electrochemical double layer (EDL) of a metal-electrolyte interface, when potential is applied on the metal by a potentiostat. We applied this method to an electrochemically clean polycrystalline gold (poly Au)-electrolyte interface and measured zeta potential for various applied potentials, pH, and concentration of the electrolyte. Specific adsorption of chloride ions on poly Au was studied by comparing measurements of zeta potential in KCl and $KClO_4$ electrolytes. In absence of specific adsorption, zeta potential was found to increase linearly with applied potential, having slope of 0.04–0.06. When Cl^- adsorption occurs, zeta potential changes the sign from positive to negative value at ~750 mV vs Ag/AgCl applied potential. Complementary cyclic voltammetry and X-ray photoelectron spectroscopy studies were conducted to determine a degree of chloride ion adsorption on a poly Au. A correlation was observed between the applied potential at which zeta potential is zero and potential of zero charge for poly Au. Ion-distribution and ionic conductivity in the diffuse layer were calculated from the measured zeta potential data using nonlinear Poisson-Boltzmann distribution.
© 2021 The Author(s). Published on behalf of The Electrochemical Society by IOP Publishing Limited. This is an open access article distributed under the terms of the Creative Commons Attribution Non-Commercial No Derivatives 4.0 License (CC BY-NC-ND, http://creativecommons.org/licenses/by-nc-nd/4.0/), which permits non-commercial reuse, distribution, and reproduction in any medium, provided the original work is not changed in any way and is properly cited. For permission for commercial reuse, please email: permissions@ioppublishing.org. [DOI: 10.1149/1945-7111/abf4aa]

Manuscript submitted December 27, 2020; revised manuscript received March 9, 2021. Published April 14, 2021. *This was paper 235 presented at the Dallas, Texas, Meeting of the Society, May 26-May 30, 2019.*

Supplementary material for this article is available online

Electric double layers (EDLs) are formed at most solid-liquid interfaces due to the difference in chemical potential of ions in the two media and electronic spillover.[1] At metal-electrolyte interface, ion distribution and ionic conductivity in the EDLs is influenced by electric potential applied on the electrode surface and electrolyte chemical composition (pH and concentration of electrolyte, concentration of specifically adsorbing ions etc.). Understanding the EDL structure is critical for optimal design of electrodes for various electrochemical devices, such as fuel cells, electrolyzers, solar-fuel generators, water desalination devices etc. In all these systems, polarized interfaces are responsible for carrying out electrochemical reactions or for storing charge in the EDLs.[2–5] Electrochemical redox reactions and specific adsorption of ions involve Faradaic charge transfer at the electrode and electrolyte interface. These Faradaic reactions are studied using well-established electrochemical techniques, such as chronoamperometry, cyclic voltammetry (CV) and electrochemical impedance spectroscopy (EIS). Ex-situ methods, such as X-ray photoelectron spectroscopy (XPS),[6] surface-enhanced infrared spectroscopy[7] have also been used to study the growth of the surface oxides and orientation of water dipoles at the metal surfaces under applied potentials. One convenient way to study ion distribution and ionic conductivity in the EDLs is to measure potential at the outer Helmholtz plane (OHP), and then use Gouy-Chapman-Stern (GCS) or modified theories[8] to calculate combined metal and adsorbed species charge, ion distribution and ionic conductivity in the diffuse layer. This potential is also called zeta potential, and it has important application in the field of electrochemistry. For example, Frumkin correction to Butler-Volmer equation uses a potential difference between the metal and the OHP as a driving force for the Faradaic reactions.[9] Zeta potential can also predict ionic conductivity in the diffuse layer of the EDL, which is important for a variety of applications, where ion transport due to the EDLs dominates over the bulk ionic transport. The ratio of the surface to bulk ionic conductivity is called Dukhin number[10] and it is a widely used quantity in understanding ion conduction inside the microfluidic systems. Ionic conductivity in the EDL is more relevant than bulk electrolyte conductivity in systems where electrochemical reactions occur within the confined environments.[11,12] Besides predicting ion distribution and ionic conductivity in the EDL, as well as redox currents, study of zeta potential also provides important conceptual information about the charging behavior of the electrode.

Zeta potential cannot be directly measured using electrochemical or ex situ surface characterization techniques mentioned above. Non-electrochemical methods are better suited for zeta potential measurements. For example, electrokinetics (streaming current/streaming potential),[10,13] dynamic light scattering (DLS),[14] atomic force microscopy (AFM),[15,16] electrochemical surface force apparatus (EC-SFA)[17] can be used to probe the EDLs. DLS is the most commonly used technique to measure zeta potential of colloidal particles in a dispersion.[18] For macroscopic substances, techniques like electrokinetics, AFM, EC-SFA are used. Electrokinetic streaming potential and streaming current techniques are suitable for precise measurement of zeta potential of macroscopic substances of different geometries (planar, granular etc.).[19] Traditional electrokinetic experiments involve solid-liquid interfaces, where surface charging takes place by ions (ionic charging) in the electrolyte. Electrokinetic measurements of zeta potential at the interface of a conductive solid with electrolyte, where potential is applied on the solid surface using an external source such as potentiostat, are non-trivial. However, zeta potential at such interfaces has been studied using non-electrokinetic techniques. Barten et al.[15] and Wang et al.[16] measured zeta potential at externally polarized polycrystalline Au (poly Au)-electrolyte interface by AFM using silica probes. Kasuya et al.[17] studied the effect of anion adsorption on zeta potential of externally polarized poly Au-electrolyte interface using EC-SFA. Both AFM and EC-SFA are surface force methods. AFM measurements are local, whereas the EC-SFA measures force over a large surface area. Force between the probe and the sample is measured as a function of their separation distance. Zeta potential is evaluated by fitting the measured force-distance data using Derjaguin-Landau-

[z]E-mail: Iryna.zenyuk@uci.edu

Verwe-Overbeek (DLVO) theory. DLVO theory can efficiently model long range double layer forces, but ambiguity arises in the vicinity of the OHP, where Van der Waals attractive forces dominate over the double layer forces.[20] Electrokientic methods (streaming current/streaming potential) are more straightforward in measuring zeta potential. Streaming potential values tend to be on the order of tens of mV, whereas streaming currents are usually small in magnitude (maximum hundreds of nA).[21,22] Streaming current measurements require sensitive and non-polarizable electrodes. Moreover, evaluating zeta potential from streaming current data requires precise knowledge of the sample-electrolyte contact area.[19] Because of these reasons, streaming potential is more frequently used to measure zeta potential of macroscopic samples. However, streaming current technique is more convenient for measuring zeta potential at metal-electrolyte interfaces. A brief explanation of this issue is provided in the Theory and Physical Modeling section.

In our earlier study,[23] a method was developed to measure zeta potential at an externally polarized metal-electrolyte interface. Au sputtered onto a copper sheet was used as a metal sample. In this and our previous study, streaming current technique was used to measure zeta potential. In this work several significant improvements in the method for zeta potential measurements are presented. Earlier work used built in Ag/AgCl electrode, just outside the microfluidic channel, to measure streaming current, which introduced several challenges. First, Ag/AgCl electrodes did not short all the streaming current transported from the microfluidic channel (as additional current was introduced due to charging metal samples), resulting in an oscillatory charging at the interface and non-monotonic charging curves. The second challenge in the earlier setup was the limitation of electrolyte selection. As Ag/AgCl/KCl is a stable electrochemical redox couple, only KCl was used. In this study, we modified the measuring set-up to be more affordable for an academic laboratory, as well as more flexible with the selection of electrolytes. The method is affordable, as it requires only pressure regulated microfluidics cell with a three-electrode electrochemical setup. Most of the electrochemistry laboratories already have three-electrode set-ups and potentiostats, and hence, the only addition that is needed is a microfluidic cell and components (for example, syringe pump, pressure transducer and sample holder with the channel for mounting metal samples). By using a Pt counter electrode commonly used for electrochemical setups, we eliminated the limitations in the choice of electrolytes, and studied the impact of electrolyte on zeta potential of Au surface with and without adsorbing ions.

In this study, the poly-Au surface was extensively cleaned using the standard pretreatment procedure for poly-Au.[24] The rigorous cleaning minimized contribution from the surface impurities and increased the reproducibility of measured data. The novel finding of this study is the effect of specific adsorption of Cl^- ions on zeta potential by comparing the measurements in Cl^- and ClO_4^- containing electrolytes. As ClO_4^- is known to be the least adsorbing anion on poly Au surface,[17,25] it was used as a baseline to understand the effect of the specific adsorption. Previous studies indicate that specific adsorption of Cl^- on poly Au occurs at high applied potentials[17,25,26] and in this study we provide in-depth investigation of this anion specific adsorption using electrokinetic method. Here the electrokinetic study is further supported with cyclic voltammetry (CV) and XPS studies. Zeta potential measurements are compared with electrokinetic and more traditional dynamic light scattering techniques for poly Au. A comparison between zeta potential values in this study and those by Barten et al.[15] using AFM technique shows good agreement. Finally, the study is concluded with a discussion of the general features and limitations of this method.

Theory and Physical Modelling

In our earlier work,[23] the structure of the EDL (without self-assembled monolayers), an exact analytical solution of non-linear Poisson-Boltzmann equation, and a complete solution of Navier–Stokes equation to find the relationship between streaming current and zeta potential were presented. Here, only salient details of descriptions and formulae are shown.

Figure 1a gives a schematic representation of the EDLs, and Fig. 1b shows the surface charge that can be calculated from the electrokientic measurements using the GCS theory. The metal surface charge consists of two contributions: i) excess or lack of electrons and is referred to as the "metal charge," and ii) adsorption of ions at the IHP. The next layer within the EDLs is OHP and it consists of partially or fully hydrated ions. Ions in this layer and beyond are hydrodynamically mobile. Poisson-Boltzmann equation determines the distribution of hydrated ions in the diffuse layer. In the streaming current experiment, a rectangular sample is mounted on the top and bottom walls of the microchannel and an electrolyte

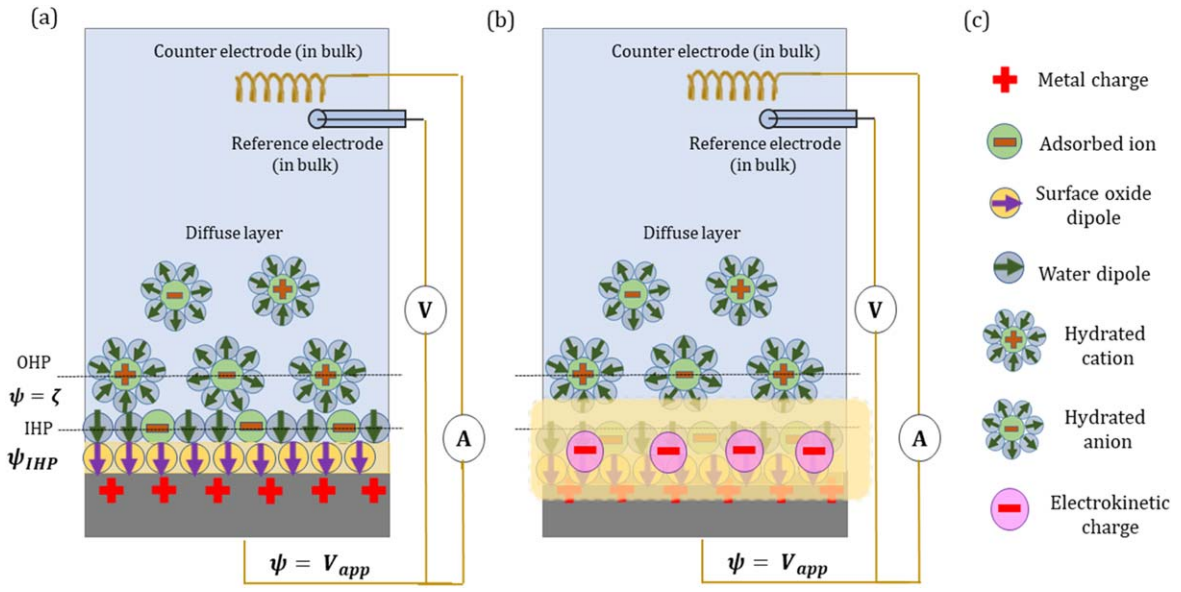

Figure 1. A schematic representation of ion distribution in the EDL when potential is applied externally on the metal. (a) A GCS model with the IHP and the surface oxide layer, (b) an EDL representation where the surface charge is shown as it is probed by electrokinetic methods, and (c) labels of all the chemical species present in the EDL. A schematic of a three-electrode set-up is shown here too. Surface dipole is drawn following the convention used in chemistry (vector points from partially positive to partially negative charge).

of known chemical composition (pH, concentration, specifically adsorbed ions etc.) is flown through the channel under various pressures. The bulk solution is electroneutral and hence the net bulk current is zero. The mobile charges in the diffuse layer give rise to the pressure-driven current, termed the streaming current (I_S). Zeta potential can be determined from the streaming current vs pressure data:[19]

$$\zeta = \frac{\eta}{\epsilon_r \epsilon_0} \frac{L}{A} \frac{dI_S}{dP} \quad [1]$$

where, L and A are the rectangular channel length and area, respectively, η and ϵ_r are the viscosity and dielectric constant of the bulk electrolyte, respectively, and P is the pressure at which the liquid is flown through the channel. The complete derivation with all the necessary approximations is given in our previous paper.[23]

As mentioned in the Introduction section, streaming potential is more frequently used in the electrokinetic experiments. During the measurement of streaming potential, lateral electric field is generated due to the lateral voltage drop across the channel. This electric field polarizes the metal cathodically on one side and anodically on the other. Faradaic current generated from this polarization exactly equals the current through the bulk metal due to the flow of electrons. Streaming potential is measured when streaming current is counterbalanced by the sum of Ohmic current through the bulk electrolyte, ionic current at the metal-electrolyte interface and Faradaic current through the bulk metal. As a result, evaluation of zeta potential from the streaming potential measurements requires quantitative analysis of the surface ionic conductivity and electron transfer kinetics at the metal-electrolyte interface.[27] Duval et al. studied streaming potential at bipolar Au-KNO_3 electrolyte interface in the presence of $Fe(CN)_6^{3-}$/ $Fe(CN)_6^{4-}$ reversible redox couple.[28] The lateral electric field, generated due to the potential difference inside the channel, complicates the interpretation of data. No such electric field is generated during the streaming current measurement, as there is no lateral potential difference along the channel. As a result, zeta potential can be evaluated directly from Eq. 1 without any corrections for the surface ion conduction or Faradaic currents. Gallardo-Moreno et al.[29] measured zeta potential at metal-electrolyte interfaces, when potential was not applied externally, using both streaming current and streaming potential methods. They concluded that after correcting for the surface and bulk conduction, zeta potential measured with streaming potential agrees well with that measured with streaming current. Similarly, Duval et al.[27] showed corrections for surface and bulk conduction for streaming potential measurements. For these reasons, streaming current method was adopted in this study to measure zeta potential at a metal-electrolyte interface. Ion distribution in the diffuse layer can be found, either analytically or numerically, by substituting zeta potential value in Poisson-Boltzmann equation. Electroneutrality at the metal-electrolyte interface results in charge balance between metal, IHP and diffuse layer:

$$\sigma_0 + \sigma_{IHP} + \int_{OHP}^{bulk} \rho_E(x)dx = 0 \quad [2]$$

where, σ_{IHP} is the charge due to ion adsorption at the IHP, the third term on the left is the surface charge density, σ_d, for a diffuse layer.[23] σ_0 is the overall charge on the metal, which is due to excess electrons, as well as surface oxides and complexes. Surface complexation reactions will be discussed in the Results and Discussion section, when change of the zeta potential with pH of the solution is discussed. For a binary symmetric electrolyte, the charge density in the diffuse layer can be analytically calculated to be:

$$\sigma_d = -(8RT\epsilon_r \epsilon_0 c^0)^{\frac{1}{2}} \sinh\left(\frac{ze\zeta}{2k_B T}\right) \quad [3]$$

where c^0 is the bulk electrolyte concentration in mol/l, z is charge number, R is ideal gas constant, T is temperature, ϵ_r and ϵ_0 are relative and absolute permittivity of water, e is the electron charge and k_B is the Boltzmann constant. Surface charge obtained from zeta potential measurements is called "electrokinetic" charge. It is defined as $\sigma_{ek} = -\sigma_d = \sigma_0 + \sigma_{IHP}$ and it is shown schematically in Figure 1b. Using charge density in the diffuse layer, one can also calculate diffuse layer ionic conductivity:[23]

$$\kappa(OHP) = \frac{F^2 z^2}{RT} \sum D_i c_i^0 exp\left(-\frac{ez_i\zeta}{k_B T}\right) \quad [4]$$

where D is the diffusion coefficient for ionic species i in electrolyte. The superscript 0 stands for quantities in the bulk solution. In both Eqs. 3 and 4, the concentration c^0 depends on the solution pH.[23]

Ion specific adsorption and solvent dipole distribution at the IHP are too complex for analytical treatment and are often modeled by phenomenological adsorption potentials.[30] There is also a degree of ambiguity in determining the metal charge. Jellium model[31,32] describes the metal charge physically, where spilled over electrons are in equilibrium with a background positive metal charge. Ionic charging at the solid-electrolyte interface is explained by various site-binding models,[30,33] where the solid forms bonds with the adsorbed H^+ and OH^- ions. The bulk concentrations of these ions play important role in the determination of the surface charge. Studies by Frumkin and Petrii[34] on potential of zero charge (PZC) of platinum group metal-aqueous electrolyte interfaces also indicate that the potential of zero total charge is more relevant in non-vacuum environments than potential of zero free charge. These studies indicate that the IHP plays a significant role in the determination of the PZC. Electrokinetic methods focus exclusively on the diffuse layer, as streaming current arises due to ion transport in this layer. Thus, the method presented here can predict the diffuse layer charge density (σ_d) and ion conductivity. Surface charge calculated from the electrokinetic measurements (referred to as "electrokinetic charge") is the "effective charge" on the surface and it is known to deviate from the charge obtained using other methods.[16,35] Surface charging models, such as complexation models have been developed, including those for Au-electrolyte interface, as reported by Duval et al.[36,37] Here, only a qualitative explanation of the electrode charging behavior based on the work of Duval et al.[36,37] will be presented, as this is not the focus of the study.

Several important assumptions implemented in this study are provided here. The GCS theory approximates hydrated ions in the diffuse layer as point charges. Consequently, dielectric constant, viscosity, diffusion constant, ionic mobility etc. in the diffuse layer are assumed to be the same as in the bulk solution. These approximations can break down in a number of situations, and interpretation of the charge-transport phenomena in these domains have been reviewed by Bazant et al.[8] and Huang et al.[38] In this study 0.1 M electrolyte was used and at this high solution concentration, the validity of the GC theory was questioned before.[39] However, Monte Carlo simulation studies by Torrie and Valleau[40] and other subsequent studies[8] showed that the GC theory predicts ion distribution in the diffuse layer accurately for 0.1 M binary symmetric electrolyte and for moderate values of zeta potential ($e\zeta \sim k_B T$). At higher electrolyte concentrations, several models predict ion concentrations to have larger length scales than the Debye length.[41,42] In these cases, the PB distribution does not give an accurate prediction of ion distribution in the diffuse layer. This fact has also been verified by the AFM studies of electrostatic screening length of ionic liquids and concentrated NaCl electrolyte.[43] Theoretical models also predict that relative dielectric constant in the diffuse layer decreases below the bulk water value of 80 with increase in ion concentration.[44] Dynamic viscosity follows the same trend.[44] Modified PB distribution models exist but are highly complex and require more experimental validation. In future, modified PB models will be considered for more accurate prediction of diffuse layer properties from the measured streaming current.

Methods

Materials and pre-experiment preparation.—ASTM I (resistivity 18.2 MOhm-cm, 2 ppb TOC) grade DI water, purified by Milli-Q Direct water purification system (Millipore Sigma) was used to prepare the solutions and cleaning of the poly Au surfaces. A 99.99% pure, 0.5 mm thick poly Au foil (Sigma Aldrich, USA) was used as the sample and a working electrode (WE). It was cleaned using the electrochemical pretreatment described by Carvalhal et al.[24] First, poly Au was mechanically polished with alumina slurry of 5 μm, 3 μm and 0.05 μm diameter in succession. After that, the foil was ultrasonicated for one minute in a DI water. Then it was put in a piranha solution (70% 1 M H_2SO_4 + 30% H_2O_2) for 15 min to remove the organic impurities. It was ultrasonicated again for one minute in a DI water. Then cyclic voltammetry (CV) was used to clean the poly Au in a 0.1 M $HClO_4$ solution between 0 to 1.2 V (RHE) at 350 mV s^{-1} for 20 cycles. After the cleaning steps, the foil was cut in half to be mounted on two sample holders. For electric connection between the potentiostat and the WE, copper wires were connected at the back side of the poly Au. Copper wires did not contact electrolyte and thus did not contaminate the measurements.

For the DLS studies, $>$ 99.9% pure poly-Au powder ($<$ 10 μm) from Sigma-Aldrich was used. It was cleaned multiple times in ASTM I water by ultrasonicating for 20 min. After that, it was put in 0.001 M KCl and $KClO_4$ electrolytes, and ultrasonicated for 15 min to form uniform dispersions. During the DLS measurements, these dispersions were ultrasonicated frequently to prevent poly-Au agglomeration.

Two types of electrolytes were used in this study. 0.1 M KCl (Sigma Aldrich, ACS reagent, 99.0%–100.5%) was mostly used as the background electrolyte. Electrokinetics community generally uses KCl electrolyte and a pair of Ag/AgCl electrodes for measuring both streaming current and streaming potential. Ag/AgCl/KCl is a stable reversible electrochemical couple and the charge transfer at the interface is well understood. While measuring streaming current/potential, one must ensure that the overpotential due to pressure driven current flow is as low as possible. For Ag/AgCl/KCl, it is less than 1 mV for 50 atm change of pressure.[45] For this reason, most of the commercial electrokinetic instruments use this combination of electrolyte and reference/counter electrode for measurements. 0.1 M $KClO_4$ electrolyte (Sigma Aldrich, ACS reagent $>$99.0%) was used for ion adsorption studies. This electrolyte has similar solution properties (viscosity, dielectric constant) to that of 0.1 M of KCl. ClO_4^- ions are known to be the least adsorbing on the Au surface,[17] and hence the effect of Cl^- adsorption on zeta potential against much less adsorbing ClO_4^- ions can be studied. $KClO_4$ has higher ionic conductivity than KCl of the same molar concentration, which improved the uncompensated resistance.

For titration, concentrated HCl and KOH (Sigma Aldrich) were used. The pH in the external liquid storage container was measured by an Ag/AgCl based pH sensor provided by Anton Paar. Ultra-high purity N_2 gas (Airgas NI-UHP 300) was used to purge electrolyte solution for 5 min before every measurement. Gamry 1010E (Gamry Instruments, PA, USA) potentiostat was used to apply potential and measure the total current. Ag/AgCl reference electrode (RE) (9.5 mm outer diameter, Pine Research, NC, USA) was used in the external electrolyte storage container. A coiled polycrystalline Platinum wire (6.5 mm OD, Pine Research, NC, USA) was used as a counter electrode (CE). For the CV analysis in $KClO_4$, Hydroflex reversible hydrogen electrode (RHE) made by Gaskatel, Germany was used.

Experimental procedure.—A schematic of the experimental set-up is shown in Figure 2, with all the major components and electric connections. Microchannel contains the poly Au sample, external liquid storage container houses the RE and CE. The pumps regulate the electrolyte flow between the external, internal liquid storage containers and a microfluidic channel. The microchannel consists of a rectangular channel, where 2 cm $\times$ 1 cm poly Au samples were mounted symmetrically (separated by $\sim$10 μm). The microchannel walls are made from polyether ether keton (PEEK) to ensure high chemical stability. SurPASS 3.0 (Anton Paar, Graz, Austria) was used to measure streaming currents for poly Au-electrolyte interface, when no potential was applied externally. The channel dimensions did not change from our earlier study.[23]

After the sample was mounted inside the microfluidic channel, the dials on the sample holder were adjusted until the gap of 140–150 μm was achieved. To ensure that the poly Au samples do not touch and do not close the channel, the resistance across the two poly Au samples was measured with multimeter. Once the channel width was established, the electrolyte was flown for five times through the channel to completely wet the WE and to equilibrate the system. Then the uncompensated electrolyte resistance (R_S) was measured using potentiostatic EIS at different electrolyte flow pressures. The EIS was conducted in a frequency range of 1000–10,000 Hz and a perturbation potential of 10 mV. In SurPASS 3.0, when the experiment is initiated the electrolyte is drawn automatically from the external storage container into a temporary internal secondary container, after which electrolyte flows through the channel, as shown schematically by Fig. 2. As a result, the ionic connection between the WE, RE and CE is established, when the electrolyte exits the channel and flows back to the external container. Chronoamperometry experiments were initiated, using V_{tot}, applied by Gamry potentiostat, when the electrolyte is connecting the channel and the external container (where the CE and RE are positioned) and were stopped when all the electrolyte has exited from the channel. The total duration of the experiment per each potential point and pressure point is about 20 s. Chronoamperometry experiments were collected across the iR-corrected potential (V_{app}) from $-$400 to 800 mV (vs Ag/AgCl) in increments of $\sim$200 mV. The liquid pressure was kept constant during each experiment and was stepped in 200 mbar intervals from 200–1000 mbar. Once the pressure and potential range is completed the pH was changed from 2 to 7 and 12.

The DLS zeta potential measurements of poly Au nanoparticles were conducted by measuring electrophoretic mobility of the charged Au particles. Horiba SZ-100 nanoparticle analyzer was used for the measurements. Colloidal dispersions of clean poly Au in 0.001 M KCl and 0.001 M $KClO_4$ were prepared. HCl and $HClO_4$ were used as titrating acids for KCl and $KClO_4$ respectively, and KOH was used as the base. During the experiment, pH was varied from 2 to 12 by manually adding base to the colloidal dispersion stored in an external container. The cuvette from which zeta potential measurements were performed, was cleaned with DI water, and then dried with air before the dispersion was changed. In the cuvette, graphite electrodes were used to apply $\pm$3 V potential and accelerate the charged Au particles. At each pH value, 5 measurements of electrophoretic mobility were conducted, and zeta potential was calculated from Henry's equation with Henry's constant value of 1.5.[18] Before the zeta potential measurements, the average size of Au nanoparticles was measured using DLS method and was found to be much higher than Debye length ($\sim$ 10 nm). So, we used Henry's constant value of 1.5. At this limit, Henry's equation reduces to Helmholtz-Smoluchowski equation.

The XPS data were measured by Kratos AXIS Supra X-ray photoelectron spectrometer with a monochromatic Al Kα. The survey spectra were acquired using 160 eV pass energy, while the high-resolution spectra of C 1 s, O 1 s were acquired using 20 eV pass energy and the high-resolution spectra of Cl 2p using 40 eV pass energy.

Equivalent circuit and data interpretation.—Figure 3 shows a schematic of the equivalent circuit description of the experimental set-up (from Figure 2). Figure 3a shows a conventional electrokinetic (EK) setup, and Figure 3b represents the modified setup (the combined electrokinetic-electrochemical setup, also shown by Figure 2). In a traditional EK setup, the sample to be studied is mounted inside a microchannel, which contains the electrolyte. A

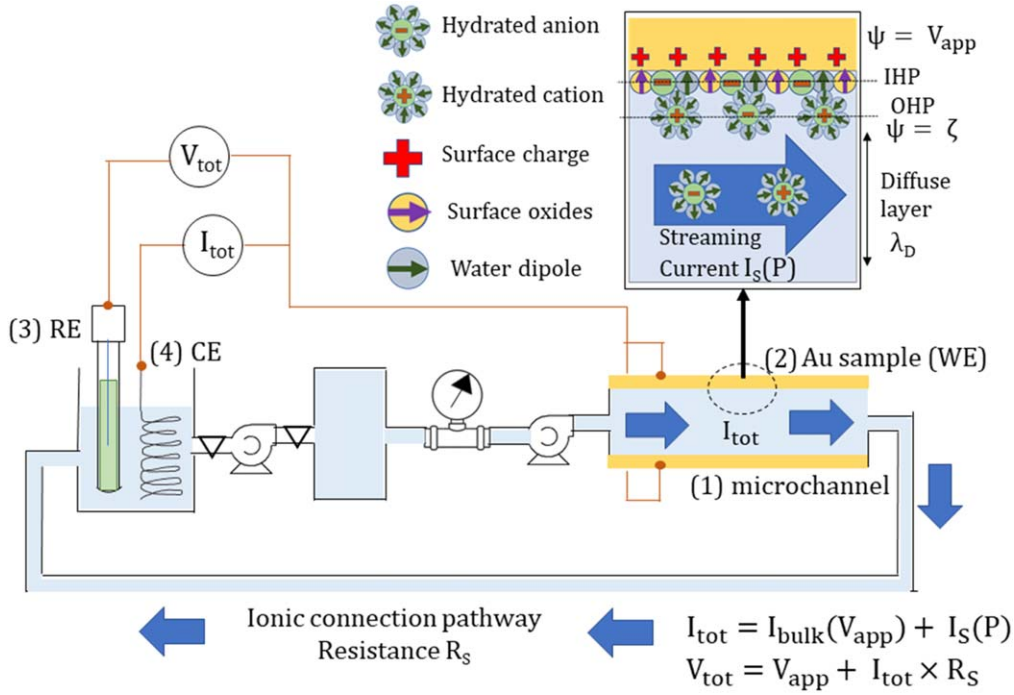

Figure 2. Schematic design of a combined electrochemical-electrokinetic setup and its principal components- (1) microchannel holding the metallic sample, (2) Au sample used for this study. This is also the working electrode (WE), (3) reference electrode (RE) in the beaker that contains the electrolyte of specific chemical composition, and (4) counter electrode (CE) that measures the total current I_{tot}. Working electrode is ionically connected to the reference and counter electrode only when the electrolyte exits the microchannel.

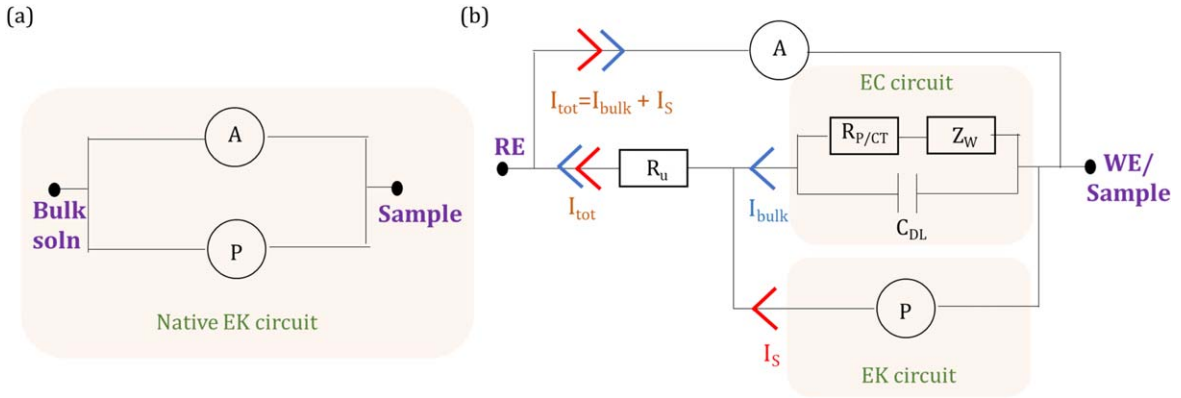

Figure 3. (a) Standard or native electrokinetic (EK) circuit to measure I_S (P), (b) equivalent circuit for a combined electrochemical (EC) and EK setup, with the native EK ammeter disconnected.

pressure-driven liquid flow is induced within the microchannel, with pressure, P. In the equivalent circuit model, P acts as the source of the streaming current (equivalent to a battery in an electrical circuit). An ammeter is used to measure the resulting streaming current. A schematic description of a conventional electrokinetic setup with all geometric details is provided in our previous paper.[23]

To measure zeta potential at the electrode-electrolyte interface when the potential is applied externally on the electrode, a 3-electrode electrochemical (EC) cell is introduced within the electrokinetic cell. The sample represents the working electrode (WE) and bulk represents the reference electrode in the EC circuit. Zeta potential is calculated from the streaming current data using Eq. 1. When potential is applied on the metal surface (WE) and electrolyte is flown simultaneously, current arises from two sources: 1) polarization of the electrode due to the applied potential and 2) ion convection in the diffuse layer by pressure driven flow (streaming current). When potential is applied on a WE in a traditional EC cell, current flows due to polarization of the electrode. This current is termed here as a "bulk current" (I_b). This current is similar to that observed in the chronoamperometry experiments. As currents from the two sources add up, the EC part (Randles circuit) must be connected in parallel to the EK part:

$$I_{tot}(V_{app}, P) = I_b(V_{app}) + I_S(\zeta(V_{app}), P) \quad [5]$$

Bulk current depends on the applied potential but it does not depend on electrolyte pressure, P. Streaming current (I_s) depends on the electrolyte pressure and on zeta potential. As zeta potential depends on the ion distribution in the EDL, which is influenced by the applied potential on the electrode, zeta potential depends on the applied potential. Therefore, streaming current implicitly depends on the applied potential. In the combined EC-EK setup (Figure 3b), the EK ammeter of the traditional EK setup (Figure 3a) is disconnected and a counter electrode (CE) used regularly in the EC experiments (coiled Pt wire) measures the total current $I_{tot}(V_{app},P)$ Zeta potential can be evaluated from $I_{tot}(V_{app},P)$ by:

$$\zeta = \frac{\eta}{\epsilon_r \epsilon_0} \frac{L}{A} \frac{dI_S}{dP} = \frac{\eta}{\epsilon_r \epsilon_0} \frac{L}{A} \frac{dI_{tot}}{dP} \quad [6]$$

The second equality holds, as the pressure dependence of the I_{tot} comes only from I_S. Section S1 in Supplementary Material contains a detailed comparison with the technique used in our previously study. Determination of the uncompensated resistance is given in section S2. Section S3 shows streaming and bulk current measurements and evaluation of zeta potential from them.

Results and Discussion

Figure 4 shows the measured zeta potential for poly Au in KCl electrolyte for various pH and concentrations of KCl from 10^{-4} to 10^{-1} M in the native electrokinetic setup (without applying potential). In general, zeta potential decreases and become more negative when pH is increased. This is explained by site-binding equilibrium[30] and is also known as ionic-charging of the electrode. For poly Au, the details of this charging mechanism was presented by Duval et al.,[36,37] and here a qualitative argument for the decrease of zeta potential with increasing pH is provided. The chemical equilibrium governs the surface charging and can be shown as:

$$\begin{aligned} MOH_2^+ &\rightleftarrows MOH + H^+ \; K_{a_1} \\ MOH &\rightleftharpoons MO^- + H^+ \quad K_{a_2} \end{aligned} \quad [7]$$

In aqueous solutions, H^+ and OH^- are the potential determining ions and they govern the surface charging behavior. In Eq. 7 M represents the metal (poly Au here) in contact with the electrolyte. The dissociation constants K_{a_1} and K_{a_2} can be determined from zeta potential ζ(pH) and titration data.[37] If pH is decreased, the number of H^+ ions in the bulk electrolyte increases. Consequently, the density of H^+ ions in the diffuse layer also increases. This drives the reaction with equilibrium constant K_{a_1} from right to left and the number of MOH_2^+ increases. The second reaction also shifts towards left to produce more MOH dipoles. As MOH is uncharged, it does not contribute to the surface charge. To balance extra positive charge of MOH_2^+ at low pH, the diffuse layer must contain more negative charge . Equation 3 shows that zeta potential must increase in this case. For increasing pH, the opposite mechanism occurs and zeta potential decreases.As shown by Figure 4, zeta potential for poly Au in KCl electrolyte flatten at high pH values (pH $>$ 8) for all KCl concentrations. This is most likely due to OH^- ion saturation at the interface at high pH and can be explained by the relative magnitude of the pK values of the chemical equilibria described by Eq. 7. The pK values are related to the dissociation rates (K_{a1} and K_{a2}) of the surface groups, where the lower pK value indicates the faster dissociation rate (reaction proceeds from left to right in Eq. 7. For Au-electrolyte interface, $pK_2 > pK_1$ (i.e. $K_{a2} < K_{a1}$), where both pK values can be determined from titration experiment. At high pH, the limiting step is the first reaction in Eq. 7, where dissociation of MOH_2^+ is slow, as the result the concentration of the MO^- does not change at certain point when the pH is further increased. And as MO^- concentration saturates, ζ becomes constant, and a plateau is observed in Figures 4 at high pH. On the other hand, no flattening in zeta potential is expected at low pH because of sluggish reaction 1 in the Eq. 7 from right to left As more protons are added to the solution (decreasing pH), the reaction keeps proceeding towards the left but at a slower rate. As MOH_2^+ increases with decreasing pH, Eq. 3 shows that ζ increases without flattening. At sufficiently low or negative pH, flattening of zeta potential with decreasing pH will most likely occur but in this study the experiments were limited to pH of 2 or higher.

Iso-electric point (IEP) is the pH value at which $\zeta = 0$. The IEP did not change significantly for different concentrations of the Cl^- ions (except for 1 mM KCl). The IEP is observed to be at around pH 5 but for 1 mM KCl it was shifted to a lower value of 4. The deviation for 10^{-3} M is most likely due to experimental error, although it is hard to pinpoint the exact reason. Consistency of the IEPs across the range of KCl concentrations suggests very mild adsorption of the Cl^- ions on the poly Au surface. For non-adsorbing electrolytes, the IEP is expected to remain the same across the range of electrolyte concentrations.[13] For low pH (range 2–4) and high pH (8–12) a trend of decreasing absolute magnitude of zeta potential was observed with the increase in electrolyte concentration. For 10^{-4} M and 10^{-1} M KCl the trend is clear, but it is not very clear between 10^{-2} and 10^{-3} M KCl. For 0.1 M KCl, which was used for applying potential externally on the Au surface, zeta potential varied between +13 to −13 mV for the pH range of 3 to 11.5. The decrease in the absolute value of zeta potential with increasing electrolyte concentration is due to thinning of the diffuse layer with the increase of ion concentration (Debye length $\lambda_D \sim c_0^{-1/2}$). For the thinner diffuse layers, the streaming current decreases and hence the measured zeta potential decreases as well. As zeta potential of the sample is sensitive to its surface conditions, the data were also compared with the previous electrokinetic studies done for poly Au sample in KCl electrolyte. The comparison is shown in SM section S4[29,46] for samples without applied potential showing a good agreement between data collected in this work and earlier studies.

Figure 4 shows the comparison of measured ζ(pH) using the EK and DLS methods for poly Au in 1 mM KCl and 1 mM $KClO_4$. Zeta

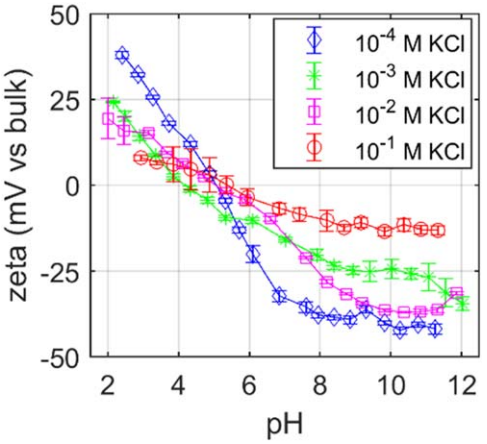

Figure 4. Zeta potential vs pH for electrochemically clean poly Au for different concentrations of KCl using the streaming current method.

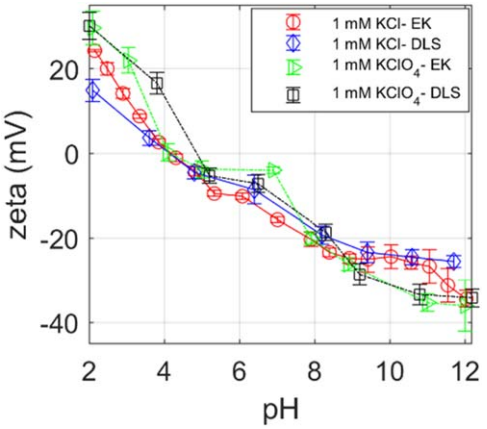

Figure 5. Comparison of zeta potential measured by the EK streaming current and the DLS techniques. Both KCl and $KClO_4$ electrolytes were used to check reproducibility.

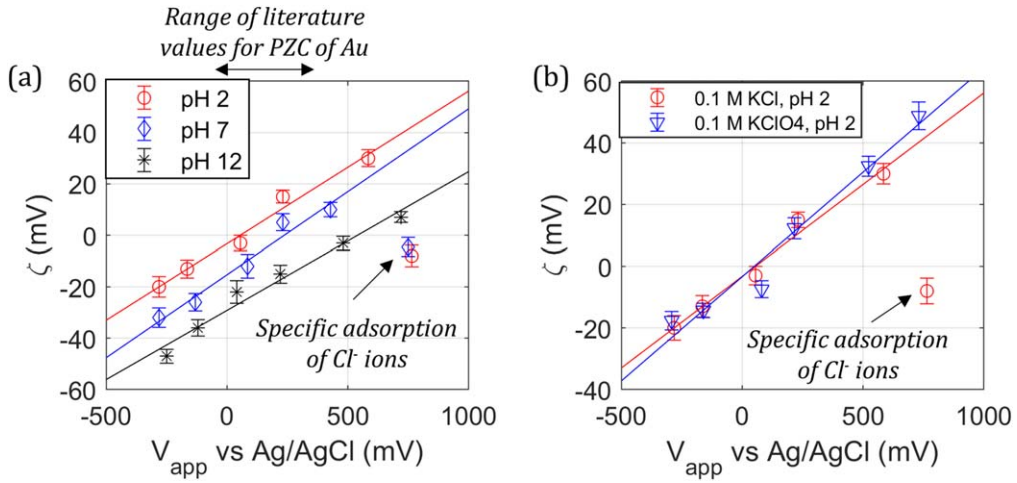

Figure 6. ζ vs V_{app} measured data and linear fits for (a) in 0.1 M KCl for three pH values, and (b) a comparison of ζ in 0.1 M KCl (pH 2 titrated with HCl) and 0.1 M $KClO_4$ (pH 2 titrated with $HClO_4$). The range of PZC values of Au shown here is obtained from literature.[49–52] The observed sudden decrease of ζ from the linear trend is due to Cl^- adsorption at around 750 mV vs Ag/AgCl reference electrode.

potential values are between 20 mV and 40 mV at pH of 2 and decrease to about −35 mV at pH of 12. Both techniques produced result in agreement with each other. No potential was applied on the metal using an external source during these measurements. Both methods showed zeta potential magnitude to be higher for 1 mM $KClO_4$ at low (2–4) pH and high (10–12) pH compared to 1 mM KCl electrolyte. This may be due to mild adsorption of Cl^- ions. As Cl^- are negatively charged, the effective charge on the electrode becomes negative. The diffuse layer must contain more positive ions to balance the extra negative charge. According to Eq. 3, ζ must become more negative which is what we observe in Figure 5.

Figure 6 shows electrokinetic zeta potential measurements of poly Au surface in electrolytes with three different pH values (2, 7 and 12), representing acidic, neutral, and alkaline environments, while potential was applied on the metal using an external potentiostat. 0.1 M KCl and 0.1 M $KClO_4$ electrolytes were used to study the Cl^- ions adsorption on the poly Au surface.[17,47,48] Figure 6a shows ζ as a function of applied potential in 0.1 M KCl. In the capacitive region (non-adsorbing region), the experimentally measured ζ was found to vary almost linearly with the applied potential. For pH 2, zeta potential increased from −20 mV at $V_{app} = -280$ mV to 30 mV at $V_{app} = 585$ mV. When V_{app} was increased to 765 mV, zeta potential dropped to −8 mV. Following a similar trend for pH 7, zeta potential increased from −32 mV at $V_{app} = -280$ mV to 10 mV at $V_{app} = 427$ mV. With further increase in V_{app} to 750 mV, zeta potential dropped to −4.5 mV. Zeta potential decrease in the case of pH 12 was not observed, where zeta potential increased from −47 mV at $V_{app} = -250$ mV to 7 mV at $V_{app} = 720$ mV.

For any given pH, increase in the zeta potential indicates the presence of more negative ions in the diffuse layer near the OHP, as can be seen from Eq. 3. Due to capacitive charging, charge on the metal surface increases with the increase in applied potential, assuming monotonic charging. More negative charge in the diffuse layer is required to maintain an overall electroneutrality in the EDL and a more positive zeta potential. The slopes for the linear region for three pH values can be calculated as: $\left.\frac{d\zeta}{d\,V_{app}}\right|_{pH=2} \approx \left.\frac{d\zeta}{d\,V_{app}}\right|_{pH=12} = 0.06$ ($\Delta\zeta =$ 6 mV for $\Delta V_{app} = 100$ mV). Similarly, $\left.\frac{d\zeta}{d\,V_{app}}\right|_{pH=7} = 0.04$ ($\Delta\zeta =$ 4 mV for $\Delta V_{app} = 100$ mV). Similar slope for zeta potential vs applied potential was observed by Barten et al.[15] in their AFM study. Figure S6 (available online at stacks.iop.org/JES/168/046511/mmedia) shows the comparison of our measured data and that reported by AFM.

Figure 6a also establishes a correlation between the PZC of poly Au and applied potential at which $\zeta = 0$ ($V_{app}(\zeta = 0)$). The PZC of poly Au depends on its crystal orientation and was measured to be between 200−500 mV (vs SHE).[17,49–52] Lecoeur et al. studied the dependence of PZC on different crystal nature of Au, and found that it is maximum for Au(111) and lower for higher index faces.[50] The authors calculated PZC from the minima found in differential capacitance curves in non-adsorbing electrolytes. In another significant study by Climent et al.[52] using laser induced temperature jump method, it was found that PZC of poly-Au was lies around 0 mV vs vs Ag/AgCl for non-adsorbing ClO_4^- containing electrolyte. However, for adsorbing SO_4^{2-} containing electrolyte, it was found to be around 200 mV vs Ag/AgCl.[52] As it is difficult to pinpoint one single value of the PZC for a polycrystalline electrode, on Figure 5a we mark a shaded region on zeta potential vs applied potential plot that represents the literature values for the PZC of various facets of Au.

From Figure 6a, the zeta potential at pH 2 and pH 7 are either very small in magnitude or zero in this applied potential range, suggesting a strong correlation between the PZC and $V_{app}(\zeta = 0)$. From the linear fits, the following were calculated: $V_{app}(\zeta = 0) \approx$ 255 mV vs SHE (55 mV vs Ag/AgCl) for pH 2, 435 mV vs SHE (235 mV vs Ag/AgCl) for pH 7, and 740 mV vs SHE (540 mV vs Ag/AgCl) for pH 12. For pH 2 and pH 7, $V_{app}(\zeta = 0)$ is within the region of electrochemically measured PZC values for Au, while for pH 12 $V_{app}(\zeta = 0)$ is higher. This is possibly due to a high oxide coverage on the Au surface at pH 12. A general trend of $V_{app}(\zeta = 0)$ is to increase with increasing pH ($\frac{dVapp(\zeta=0)}{dpH} > 0$). The density of surface adsorbed M O^- groups increases with increasing pH. To compensate the negative charge, higher potentials must be applied on the electrode. Hence, the $V_{app}(\zeta = 0)$ also increases with the increase in pH. In the absence of any specific adsorption, $V_{app}(\zeta = 0)$ should be close to the PZC.

The sudden decrease in zeta potential values at high applied potentials is observed in Figure 6a and is due to the specific adsorption of the Cl^- ions. As Cl^- ions are negative, specific adsorption of these ions decreases the effective charge density on the metal surface and shifts it negatively. To balance the overall negative surface charge, more positive ions are attracted to the diffuse layer. For such a scenario Eq. 3 indicates that zeta potential must be negative. Change in the zeta potential due to specific ion adsorption on the surface has been extensively studied in water filtration systems, where ion adsorption from feed water is controlled largely by surface charge.[53] Here the effect of Cl^- adsorption in pH 12 electrolyte was not observed, possibly because most metal sites are covered by oxides and hydroxides.

To confirm the observation of strong adsorption of Cl^- ions, zeta potential measurement were carried in 0.1 M $KClO_4$ in the same

applied potential range. ClO_4^- ion is known to be the least adsorbing anion on poly Au surface.[17] Zeta potential vs V_{app} in KCl and $KClO_4$, both in pH 2 are shown in Figure 6b. The KCl solution was titrated with HCl, and the $KClO_4$ solution was titrated with the $HClO_4$. For $V_{app} < 600$ mV (vs Ag/AgCl) zeta potential in both electrolytes was very similar, indicating that electrode charging behavior does not change significantly with ionic species in the solution if those ions do not adsorb strongly. Moreover, Cl^- adsorption on Au surface even at 0.1 M concentration is not significant for $V_{app} < 750$ mV vs Ag/AgCl. At around $V_{app} = 750$ mV, zeta potential in KCl decreased approximately by 60 mV from the projected value and became −9 mV, whereas in $KClO_4$ for $V_{app} = 680$ mV, $\zeta \sim 44$ mV. Specific adsorption of Cl^- ions around the same applied potential was previously reported in literature [17,25,47] and here specific adsorption of Cl^- ions is further studied with CV and XPS.

Figure 6a shows the CVs in two electrolytes: 0.1 M $KClO_4$ at pH 2 titrated with $HClO_4$, and 0.1 M KCl at pH 2 titrated with HCl. In KCl, an onset of high oxidative current at 800 mV vs Ag/AgCl was observed, which is due to the specific adsorption of Cl^- ions. The current in $KClO_4$ is orders of magnitude lower compared to KCl, and the CV in the $KClO_4$ is shown as an inset in Figure 6a. The current in 0.1 M KCl reaches a maximum of 10 mA at 1.3 V. Close to 1.1 V RHE current is about 2 mA and this potential translates to approximately 775 mV vs Ag/AgCl after considering 120 mV correction for pH 2. The range for the oxidation current observed in the CV matches the potential range in Figure 6, where zeta potential decrease was observed and hence the CV data is supporting the Cl^- adsorption argument. The amount of charge transferred between 800 mV and 1350 mV from the CV data was 27.1 mC cm^{-2}. The chloride adsorption also appears to be irreversible as the positive oxidation peak is observed without the negative reduction peak (desorption of Cl^-) in the reverse sweep during CV.

Figure 7b show XPS spectra of chloride adsorption on poly Au. Three samples were prepared for the study: 1) poly Au immersed in KCl without any applied potential for 1 h, 2) poly Au under $V_{app} = 800$ mV vs Ag/AgCl in 0.1 M $KClO_4$ solution for 1 h, and 3) poly Au under 800 mV vs Ag/AgCl in 0.1 M KCl for 1 h. pH 2 was maintained in all the solutions. After the potentiostatic experiments, the samples were rinsed with DI water and then dried for an hour. XPS was performed to determine the chemical species on the sample surfaces. High-resolution XPS spectra of Cl 2p were collected. The data shown here were corrected by background subtraction and were normalized. For metal chlorides, binding energy of Cl $2p_{3/2}$ electrons is ∼199 eV.[54] In Figure 7b, the Cl $2p_{3/2}$ peak at 199 eV is stronger in KCl ($V_{app} = 800$ mV vs Ag/AgCl) than the other two samples, which qualitatively shows the existence of chemisorbed Cl^- ions on the metal. Existence of Cl^- peak on all the samples suggests mild adsorption of the anion on poly-Au surface independent of externally applied potential. This peak could also be due to residual Cl^- ions that could not be removed from the surface with DI water rinsing and drying during sample preparation step.

The $\zeta(V_{app})$ from Figure 6 was used to evaluate and plot the charge density and the ionic conductivity at the OHP using Eqs. 3 and 4, respectively, as shown by Figure 8. Figure 8a shows the charge density at the OHP and Figure 8b shows the ratio of the ionic conductivities at the OHP to that in the bulk. The bulk ionic conductivity for 0.1 M electrolyte was ∼ 1000 mS m^{-1} and it also depends on pH. The projected values based on the linearly fit $\zeta(V_{app})$ from Figure 5 were also plotted. The linear fit excluded the specific adsorption of the Cl^- as its purpose was to see the trend in capacitive charging region.

Positive zeta potential indicates the presence of the net negative charge near the OHP, and the opposite is true for the negative zeta potential. When there is no Cl^- adsorption, as in Figure 6a, the zeta potential increases with the increase in applied potential for a given pH. For this case, OHP charge must be more negative and Figure 8a shows that diffuse layer charge becomes smaller and then more negative as applied potential increases. Figure 8b shows that the ratio of the OHP to the bulk conductivities is always greater than 1. $|\zeta| > 0$ indicates that the ion density at the OHP is higher than that in the bulk and Figure 8b shows that away from the $\zeta = 0$ region, ionic conductivity at the OHP is higher than that of the bulk. The ratio of ionic conductivities is higher for pH 12 compared to the other pH, reaching 2.75 value at near −220 mV. For pH 12, $\zeta<0$ for most of the V_{app} values. Negative zeta potential attracts positive ions at the OHP. H^+ ions have the highest ionic mobility and the highest equivalent conductance, $\lambda_{H+} = 349.8$ S cm^2 $equiv^{-1}$. As a comparison, the equivalent conductance of OH^- ions is 1.8 times lower ($\lambda_{OH-} = 197.6$ S cm^2 $equiv^{-1}$). Consequently, ionic conductivity at the OHP increases at pH 12. The ratio of the OHP/bulk conductivities in this paper are lower than what was found in our previous paper.[23] Here, a high concentration of electrolyte (0.1 M KCl) was used, where the bulk ionic conductivity is higher than the electrolyte used in our earlier work (0.001 M KCl). The magnitude of zeta potential did not change significantly with the concentration of the electrolyte (tens of mV). As a result, the OHP conductivity values remain almost the same, but the bulk electrolyte conductivity for this study is higher than that in the previous one. Hence, the ratio of the OHP to the bulk conductivity values reported in this work are typically lower by a factor 2–3 compared to the ratio previously reported by our group.[23] For lower bulk electrolyte concentrations, the ratio of conductivities is higher.

The section is concluded by commenting on the limitation of the combined EC-EK method introduced in this study. The main

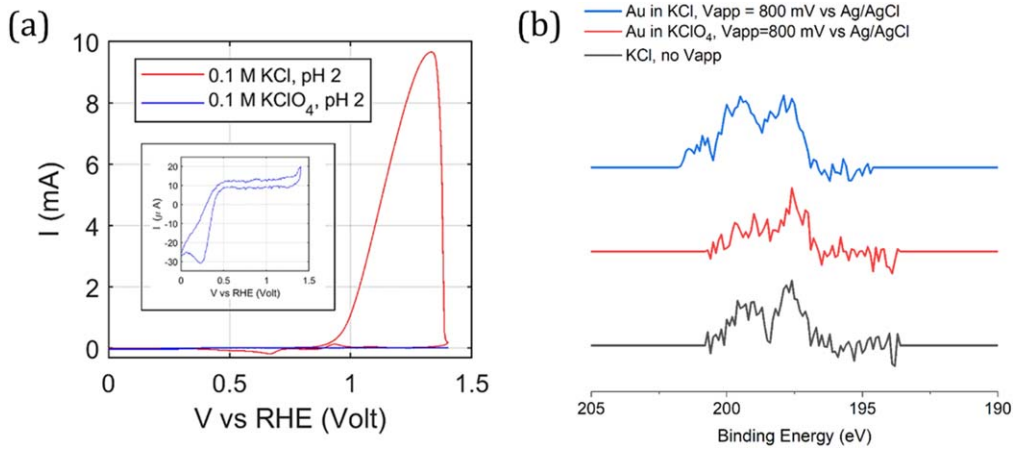

Figure 7. CV and XPS to support the hypothesis of Cl^- adsorption on poly-Au surface. (a) CV in 0.1 KCl showing oxidative current starting at 0.9 V vs RHE. CV in 0.1 M $KClO_4$ is shown as an inset. (b) XPS of poly Au in KCl (800 mV vs Ag/AgCl) shows stronger Cl $2P_{3/2}$ peak than in $KClO_4$ (in 800 mV vs Ag/AgCl) and KCl. XPS counts were corrected for background and normalized with the maximum intensities to 1. All the electrolytes were titrated to pH 2.

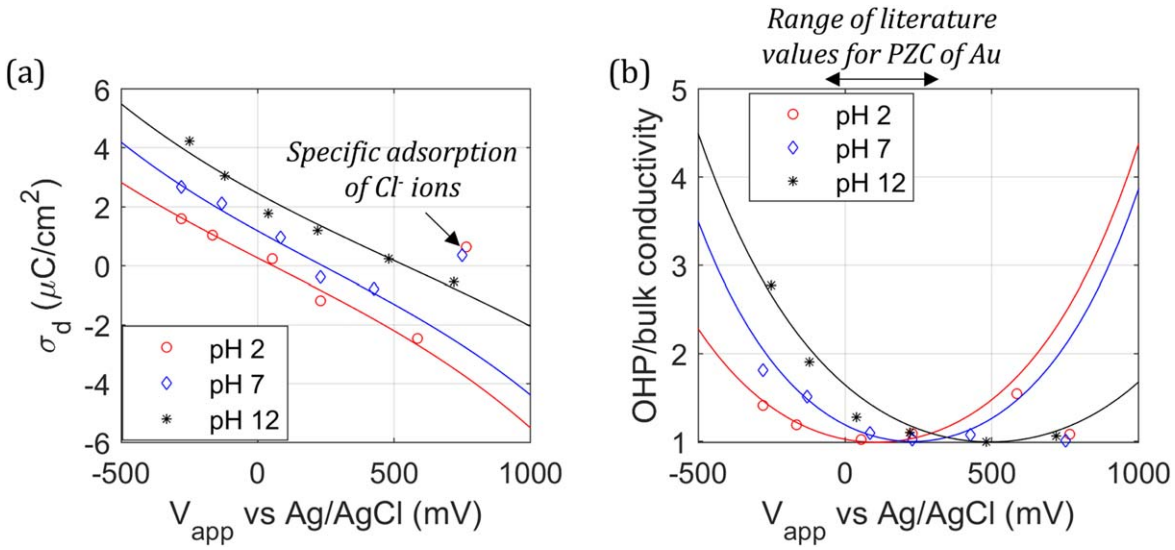

Figure 8. Experimental data and analytical calculations for zeta potential measurements in 0.1 M KCl, (a) OHP charge density vs V_{app} and (b) ratio of ion conductivities at the OHP to the bulk vs V_{app}, for three pH values. The Cl^-specific adsorption is shown in (a) and the range for the PZC values from Refs. 49–52 is shown in (b). The lines show the projected values based on linear fit $\zeta(V_{app})$ from Figure 5.

limitation is due to the spatial distancing of the microchannel from the EC unit, which creates a large uncompensated resistance, R_S. High V_{app} are difficult to apply (for example to see the double layer effect of surface oxides) because the iR drop becomes large, and as a result, the total potential required to get the target V_{app} exceeds the maximum voltage applicable by a potentiostat. However, the electrolyte flow path can be shortened to reduce R_S. Another limitation of the method is that it cannot be applied to a case where gas bubbles are formed as reaction byproduct. Gas bubbles inside the microchannels significantly alter the resistivity and the liquid flow and hamper the streaming current measurements. This method can be successfully applied only in the capacitive or pseudo-capacitive region of the applied potential range.

Conclusions

A generic, reproducible, and flexible method was developed to measure zeta potential of a metallic surface under applied potentials by combining electrochemical and electrokinetic techniques.

A regular three electrode electrochemical cell was combined with a pressure regulated microfluidic unit and the streaming current was measured using a regular counter electrode (CE) in the electrochemical cell. Zeta potential was measured for various applied potentials and pH values on polycrystalline Au surfaces. The method was validated against the DLS data, where good agreement between zeta potential measured with streaming current and with DLS was shown for poly Au in 1 mM of KCl and $KClO_4$. Capacitive charging (potential dependent) and ionic charging (pH dependent) behavior at the poly Au-electrolyte interface was found to be similar for Cl^- and ClO_4^- ions when there is no specific adsorption. With increase in applied potential from −250 to 600 mV (vs Ag/AgCl) zeta potential increased for acidic, neutral, and basic pH. Potential at which $\zeta \sim 0$ ($V_{app}(\zeta = 0)$) was found to be in a good correlation with the electrochemically measured PZC of gold. Comparing zeta potential measurements in adsorbing KCl and non-adsorbing $KClO_4$ electrolytes, Cl^- specific adsorption was detected at >750 mV applied potential. Zeta potential showed a decrease by 60 mV from the value predicted by a linear fit to zeta potential vs applied potential plot at 765 mV applied potential at pH of 2. When performing the same measurement in a non-adsorbing $KClO_4$ electrolyte, zeta potential increased linearly, when applied potential increases from 600 to 800 mV. Electrochemical cyclic voltammetry data showed a high oxidative current for poly Au in KCl electrolyte with onset potential of 800 mV vs Ag/AgCl, confirming specific adsorption of Cl^- ions to be the reason for zeta potential decrease in KCl electrolyte. Furthermore, high-resolution XPS spectra of Cl 2p showed the Cl $2p_{3/2}$ peak at 199 eV to be higher in KCl (V_{app} = 800 mV vs Ag/AgCl) than the other two samples without applied potential in KCl and $KClO_4$. Zeta potential values were fit to calculate the charge density and ionic conductivity in the diffuse layer. The charge density was found to vary between −2.3 to 4 $\mu C\ cm^{-2}$, reaching the maximum at $V_{app} = -240$ mV and pH 12. The OHP charge density decreased with increasing applied potential, as one would expect from the GC theory. The ratio of the conductivities at the OHP vs that in the bulk solution was found to vary between 1 and 2.8, with the maximum value of 2.8 at $V_{app} = -240$ mV and pH 12.

Acknowledgments

We would like to acknowledge the funding source NSF CAREER award 1652445. We thank Ying Huang for collecting XPS data, Ms. Amber Truong for helping us collect some supportive data, Dr. Andrea Perego for helping with experimental troubleshooting, Dr. Tristan Asset on directions regarding electrode cleaning procedure, Prof. Hickner's group, at Penn State University for early assistance with the set-up. Finally, we thank Christopher Liu for helping us prepare the manuscript. The DLS work was done at the HIMaC^2's Analytical Laboratory, a user facility operated by the Horiba Institute for Mobility and Connectivity, University California, Irvine.

ORCID

Prantik Saha https://orcid.org/0000-0001-9417-6872
Iryna V. Zenyuk https://orcid.org/0000-0002-1612-0475

References

1. W. Schmickler, *Chem. Rev.*, **96**, 3177 (1996).
2. I. V. Zenyuk and S. Litster, *J. Phys. Chem. C*, **116**, 9862 (2012).
3. I. V. Zenyuk and S. Litster, *ECS Trans.*, **58**, 27 (2013).
4. M. R. Singh, K. Papadantonakis, C. Xiang, and N. S. Lewis, *Energy Environ. Sci.*, **8**, 2760 (2015).
5. M. A. Modestino, S. M. H. Hashemi, and S. Haussener, *Energy Environ. Sci.*, **9**, 1533 (2016).
6. M. Wakisaka, Y. Udagawa, H. Suzuki, H. Uchida, and M. Watanabe, *Energy Environ. Sci.*, **4**, 1662 (2011).
7. K. Ataka, T. Yotsuyanagi, and M. Osawa, *J. Phys. Chem.*, **100**, 10664 (1996).
8. M. Z. Bazant, M. S. Kilic, B. D. Storey, and A. Ajdari, *Adv. Colloid Interface Sci.*, **152**, 48 (2009).
9. P. M. Biesheuvel, M. van Soestbergen, and M. Z. Bazant, *Electrochim. Acta*, **54**, 4857 (2009).

10. A. V. Delgado, F. González-Caballero, R. J. Hunter, L. K. Koopal, and J. Lyklema, *J. Colloid Interface Sci.*, **309**, 194 (2007).
11. A. Avid and I. V. Zenyuk, *Curr. Opin. Electrochem.*, **25**, 100634 (2021).
12. M. Fichtner, *Phys. Chem. Chem. Phys.*, **13**, 21186 (2011).
13. R. J. Hunter, *Zeta Potential in Colloid Science: Principles and Applications* (Academic, New York) 3rd ed., p. 386 (1988).
14. J. D. Clogston and A. K. Patri, *Zeta potential measurement*, ed. S. E. McNeil (Humana Press, Totowa, NJ) p. 63 (2011).
15. D. Barten et al., *Langmuir*, **19**, 1133 (2003).
16. J. Wang and A. J. Bard, *J. Phys. Chem. B*, **105**, 5217 (2001).
17. M. Kasuya et al., *J. Phys. Chem. C*, **120**, 15986 (2016).
18. S. Bhattacharjee, *J. Control. Release*, **235**, 337 (2016).
19. C. Werner, H. Körber, R. Zimmermann, S. Dukhin, and H.-J. Jacobasch, *J. Colloid Interface Sci.*, **208**, 329 (1998).
20. B. W. Ninham, *Adv. Colloid Interface Sci.*, **83**, 1 (1999).
21. R. M. Hurd and N. Hackerman, *J. Electrochem. Soc.*, **102**, 594 (1955).
22. D. Erickson and D. Li, *J. Colloid Interface Sci.*, **237**, 283 (2001).
23. P. Saha, C. Nam, M. A. Hickner, and I. V. Zenyuk, *J. Phys. Chem. C*, **123**, 19493 (2019).
24. R. F. Carvalhal, R. Sanches Freire, and L. T. Kubota, *Electroanalysis*, **17**, 1251 (2005).
25. T. Pajkossy, T. Wandlowski, and D. M. Kolb, *J. Electroanal. Chem.*, **414**, 209 (1996).
26. Z. Shi and J. Lipkowski, *J. Electroanal. Chem.*, **403**, 225 (1996).
27. J. F. L. L. Duval and H. P. van Leeuwen, *Adv. Colloid Interface Sci.*, **275**, 102074 (2020).
28. J. F. L. Duval, G. K. Huijs, W. F. Threels, J. Lyklema, and H. P. van Leeuwen, *J. Colloid Interface Sci.*, **260**, 95 (2003).
29. A. M. Gallardo-Moreno, V. Vadillo-Rodríguez, J. Perera-Núñez, J. M. Bruque, and M. L. González-Martín, *Phys. Chem. Chem. Phys.*, **14**, 9758 (2012).
30. D. E. Yates, S. Levine, and T. W. Healy, *J. Chem. Soc. Faraday Trans. 1 Phys. Chem. Condens. Phases*, **70**, 1807 (1974).
31. W. Schmickler and D. Henderson, *J. Chem. Phys.*, **80**, 3381 (1984).
32. W. Schmickler, *Chem. Phys. Lett.*, **99**, 135 (1983).
33. J. A. Davis and J. O. Leckie, *J. Colloid Interface Sci.*, **67**, 90 (1978).
34. A. N. Frumkin and O. A. Petrii, *Electrochim. Acta*, **20**, 347 (1975).
35. J. Lyklema, *Colloids Surfaces A Physicochem. Eng. Asp.*, **376**, 2 (2011).
36. J. Duval, J. Lyklema, J. M. Kleijn, and H. P. van Leeuwen, *Langmuir*, **17**, 7573 (2001).
37. J. Duval, J. M. Kleijn, J. Lyklema, and H. P. van Leeuwen, *J. Electroanal. Chem.*, **532**, 337 (2002).
38. Y. Gao, J. Huang, Y. Liu, and S. Chen, *Curr. Opin. Electrochem.*, **13**, 107 (2019).
39. J. J. López-García, J. Horno, and C. Grosse, *Phys. Rev. Fluids*, **4**, 103702 (2019).
40. G. M. Torrie and J. P. Valleau, *J. Chem. Phys.*, **73**, 5807 (1980).
41. I. Borukhov, D. Andelman, and H. Orland, *Phys. Rev. Lett.*, **79**, 435 (1997).
42. M. S. Kilic, M. Z. Bazant, and A. Ajdari, *Phys. Rev. E*, **75**, 21502 (2007).
43. A. M. Smith, A. A. Lee, and S. Perkin, *J. Phys. Chem. Lett.*, **7**, 2157 (2016).
44. J. J. López-García, J. Horno, and C. Grosse, *Phys. Rev. Fluids*, **4**, 103702 (2019).
45. K. S. Spiegler, *Desalination*, **15**, 135 (1974).
46. M. Giesbers, J. M. Kleijn, and M. A. Cohen Stuart, *J. Colloid Interface Sci.*, **248**, 88 (2002).
47. A. Kolics, A. E. Thomas, and A. Wieckowski, *J. Chem. Soc. Faraday Trans.*, **92**, 3727 (1996).
48. G. Horányi, E. M. Rizmayer, and P. Joó, *J. Electroanal. Chem. Interfacial Electrochem.*, **152**, 211 (1983).
49. A. Hamelin, *J. Electroanal. Chem.*, **386**, 1 (1995).
50. J. Lecoeur, J. Andro, and R. Parsons, *Surf. Sci.*, **114**, 320 (1982).
51. A. Hamelin and J. Lecoeur, *Surf. Sci.*, **57**, 771 (1976).
52. V. Climent, B. A. Coles, and R. G. Compton, *J. Phys. Chem. B*, **106**, 5258 (2002).
53. J. L. Reyes Bahena, A. Robledo Cabrera, A. López Valdivieso, and R. Herrera Urbina, *Sep. Sci. Technol.*, **37**, 1973 (2002).
54. A. V. Naumkin, A. Kraut-Vass, C. J. Powell, and S. W. Gaarenstroom, *National Institute of Standards and Technology (U.S.)* (2012).